

PRINTING HYDROPHOBIC STAINLESS STEEL GRAPHENE COMPOSITES

M. O'Donnell*, J. Budan*, J. McGuire*, P. Jalagam*, Achyuth Kulkarni*, and T.Y. Ansell*,[!]

* Department of Mechanical and Aerospace Engineering, Naval Postgraduate School
[!] Corresponding Author, E-mail: troy.ansell@nps.edu

Abstract

Hydrophobic surfaces have low surface energies, which prevents water droplets from wetting the surface. Metals typically have high surface energies leading to highly wettable, hydrophilic behavior. Nano-structuring metallic surfaces could be a way of making a metallic surface hydrophobic potentially leading to improved corrosion resistance, drag reduction, etc. 3D-printing a metal matrix nanocomposite maybe a scalable method to fabricate hydrophobic metals. Graphene nanoplatelets (GNP) were mixed with 316L stainless-steel (SS) powder and printed on a selective laser melting platform. The composite samples included 0, 1, 2, and 3 vol% GNP. Initial printing jobs ran into some issues that were addressed by adding a vibration source and aluminum foil to the inside of the powder hopper. Additionally, energy density was set higher than 60 J/mm^3 to avoid lack of fusion issues. Printing of small and large plates of composite samples was performed at energy densities starting from 60 J/mm^3 going up to 100 J/mm^3 . As-printed composite sample surfaces consistently exhibited hydrophobic behavior with contact angles exceeding 90° . After polishing, the surfaces exhibited hydrophilic behavior. What is compelling; however, is that while contact angles for pure SS was as expected, i.e., angles $< 80^\circ$, the composite samples showed angles between 80° and 90° , drawing closer to 90° with an increase in GNP.

Introduction

Corrosion is an ever-present issue for industry, militaries, and the modern world. It has been estimated that corrosion directly costs the global economy approximately six trillion USD, which is a little over 6% global gross domestic product [1]. Although an estimated 15 – 35% of this cost can potentially be avoided by implementing and following corrosion control practices, that still leaves a significant cost due to corrosion [2]. From the perspective of corrosion engineers and materials chemists, solutions to mitigate corrosion includes the use of corrosion resistant alloys like stainless steel; application of cathodic protection like attaching zinc (sacrificial anode) onto a steel hull; or coating a metallic surface with paints containing corrosion inhibitors. Each of these schemes have advantages and disadvantages. Instead, would it be possible to prevent wetting of a metallic surface by making that surface hydrophobic? One possible way would be to integrate nanoparticles like graphene into the surface of the metal.

Graphene is a two-dimensional carbon polymorph with a hexagonal honeycomb-like atomic structure. A single layer of graphene, considered the thinnest contiguous material, has a thickness of one carbon atom (0.34 nm). The material is considered one of the strongest materials known, with an average tensile strength of 130 GPa [3]. Combined with graphene's low density of 2.27 g/cm^3 , graphene has one of the highest strength-to-weight ratios. Despite its impressive properties, there is a lack of direct application of graphene, due in part to the relatively high cost

of production. The cost has been brought down by producing graphene nanoplatelets (GNP) instead of single graphene sheets. As the name implies, a GNP is a thin, flat section of graphite and can be thought of as tens or hundreds of graphene sheets kept together. There also has been limited commercialization of graphene-based composite materials. One problem has been the difficulty in integrating graphene into a matrix of another material. Some examples of integrating graphene and GNPs in possible applications include the creation of antimicrobial paper [4]. The experiment showed bacterial cultures were effectively eliminated after a short incubation period on the graphene-infused paper. In other work by Zhou et al., chemical vapor disposition was used to adhere graphene nanoplatelets to the surface of 316 L stainless-steel used in the growth of bone marrow cells [5]. Another potential application of graphene maybe in coating of metallic surfaces for corrosion protection.

Like its derivative, carbon nanotubes (CNT), graphene exhibits hydrophobicity, or the non-wetting of a surface by water [6]. The terms hydrophobicity (“water fearing”) and hydrophilicity (“water loving”) are defined by how well water droplets adhere to a surface. When the angle between a water droplet and a surface exceeds 90° , that surface is considered hydrophobic. In nature, many plants like the leaf of a Lotus plant are hydrophobic. This behavior is used to clean the surface of leaves. In engineering, researchers have attempted to fabricate hydrophobic surfaces, including metallic surfaces like stainless-steel (SS) through a variety of methods. Song et. al. demonstrated a technique where a polymethylmethacrylate (PMMA)-graphene film was transferred onto a SS surface. The surface was shown to be superhydrophobic, where contact angles were higher than 150° [7]. Typically, making metallic surfaces hydrophobic requires complicated and labor-intensive laser ablating or laser shot peening. Of course, applying a hydrophobic polymeric coating is possible and has been done. The polymers in question, like PMMA, require the application of toxic chemicals like fluorosilane to make hydrophobic. An alternative route maybe to print stainless-steel, which is composited with GNPs.

Selective laser melting (SLM) is a laser powder bed fusion technique where a layer of powder (typically metal) is deposited on a print bed and then a laser melts the powder following a digital model. Once the layer of the model has been traced by the laser, the next layer of powder is deposited and the process repeats. So, SLM is a layer-by-layer print process. Printing of hydrophobic SS samples with CNTs have been performed. Yin et. al. printed, by SLM, SS with 1 wt% (~3.6 vol%) CNTs and found increased hardness and reduced wear rate over pure SS [8]. The authors have also demonstrated printing of 316L SS with CNTs via SLM [9]. Stainless-steel was printed with up to 2 vol% CNT with a demonstration of near hydrophobic behavior when CNT content increased above 1 vol%. At 2 vol% CNTs with a printing energy density of 80 J/mm^3 , contact angles reached 88° . The goal of this research was to first print 316L SS samples composited with GNPs. Then study the effect of the GNPs on the wetting behavior of water on the surface of the printed samples. The printing energy density will be varied to study the effect on particle fusion and the melt pool structure.

Experimental

In this section, the process of printing SS-GNP composite parts is laid out. The process starts with powder processing followed by printing and sample preparation for characterization. 316L SS powder was obtained from Electro Optical Systems (EOS GmbH, Germany). The GNPs

were procured from XG Sciences (MI, USA). The GNPs had an average thickness between 6 – 8 nm and an average diameter of 15 μm . The SS and GNP powders were mixed in a high energy ball mill (8000D Mill; SPEX; NJ, USA) using 3.0 mm stainless-steel milling media at a ball-to-powder ratio of 1:5 by mass. Each composite powder was mixed in cycles of 5 minutes on and 5 minutes off over 5 total cycles. Table 1 lists the names of the powders milled prior to printing. Note that the pure stainless-steel powders were not milled. Further, changes to hydrophobic behavior with a change in energy density was explored and so samples of each powder were printed with different energy densities. To track this, the density was tacked on the end of the powder name. For example, the 2 vol% GNP powders printed with an energy density of 80 J/mm³ will be referred to as 2GNPSS-80.

Table 1. Powder names with GNP vol% and masses of SS and GNP powders.

Powders	GNP vol%	Mass SS (g)	Mass GNP (g)
SS	-	50.00	-
1GNPSS	1	49.86	0.14
2GNPSS	2	49.72	0.28
3GNPSS	3	49.58	0.42

Once milling was complete, prepared powders were placed in an oven set to between 75 and 80 °C to keep the powders dry. The dry, milled powders were printed in an EOS M100 printer. Samples were printed at energy densities ranging from 60, 67 (the default setting for the printer), 80, 90, and 100 J/mm³. Print setting for the different energy densities is listed in Table 2. The layer thickness in all cases was set to 0.02 mm. All samples were printed onto a 316L SS build plate that was heated. Printing took place in an inert argon atmosphere.

Table 2. Printer settings for the different energy densities.

Energy Density [J/mm³]	Power [W]	Laser Velocity [mm/s]	Hatch Spacing [mm]
60	77.1	917	0.07
67 (Default)	77.1	827	0.06
80	76.8	800	0.07
90	76.8	711	0.06
100	79.8	665	0.06

Two different models were printed. One model is shown in Figure 1a with the printed result shown in Figure 1b. This model had a 20 mm square surface area. A smaller square model was also printed with the same 2 mm thickness but with a 10 mm square surface. Support structures were added to the models using Magics 3D Print software (Materialise; Leuven, Belgium). In addition to the default supports, cone supports were added to the models to prevent warping. Printed samples were removed from the 316L SS build plate by water jet that cut through the support structures.

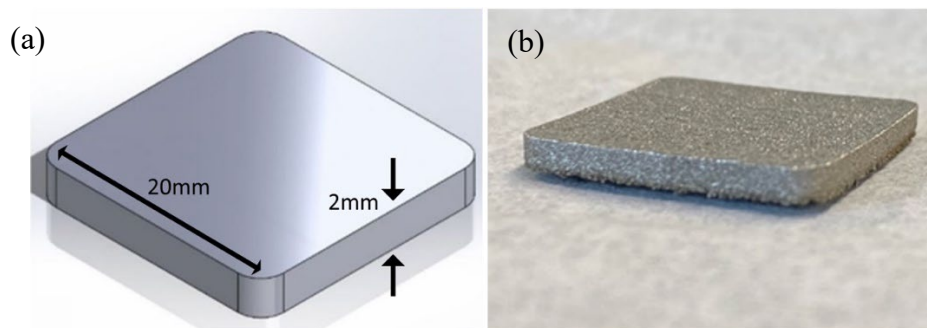


Figure 1. (a) CAD model for the large plate samples, and (b) a printed large plate sample.

After removal from the build plate, samples underwent characterization of surface roughness, contact angle, and the microstructure in that order. Surface roughness was determined using optical profilometry. A Zygo New View 7100 was used for the profilometry. Each sample had a 3 mm x 3 mm square area profiled. Because surface area affects the hydrophobic/hydrophilic behavior of a surface, samples were profiled as-printed; contact angles measured; polished using 320-, 500-, and 1200-grit SiC paper; profiled again; and then a final contact angle measurement.

Sessile drop contact angle measurements were made using a Mobile Surface Analyzer (MSA, Krüss Scientific, Germany). Due to an issue with the liquid dispenser in the MSA, a Fisherbrand Elite micropipette (Thermo-Fisher Scientific; MA, USA) was used to dispense approximately 2.0 mL of distilled water on the sample surfaces. After the droplet was deposited on the surface, the MSA was positioned over the droplet and contact angles measured. Each sample had contact angle measured for five droplets both before and after polishing.

Before microscopy, samples were cut using a high-speed sectioning saw. The cross-sections were mounted in a slow curing epoxy resin (Epofix; Struers Inc.; Ballerup, Denmark) and then underwent standard metallurgical sample preparation. After polishing, cross-sections were etched with V2A etchant (119 mL HCl, 12 mL HNO₃, 119 mL H₂O) at room temperature. The V2A etchant is a good etchant for austenitic stainless steels like 316L SS. The V2A etchant was applied by swap rather than by immersion. A cotton applicator saturated with the acid was pressed onto the sample surface twice for 30 seconds. Optical microscopy was performed on a Nikon Epiphot 200 inverted optical microscope. Electron microscopy was performed on a Helios 5-UX scanning electron microscope (SEM, Thermo-Fisher Scientific; MA, USA). SEM imaging was performed using both an Everhart-Thornley detector and an in-column detector.

Results & Discussion

The following shows our results. Hydrophobicity was demonstrated on as-printed composite samples but when polished, the surfaces were shown to be hydrophilic. Despite this, addition of GNPs to 316L-SS appear to reduce the wettability of the printed metallic surfaces. Figure 2 shows powders that were used for printing. The as-received SS powders (Fig. 2a) showed a bimodal particle size distribution with a generally spherical morphology. Upon milling with GNPs, SS particles exhibited limited deformation and mechanical welding. Seen in Figure 2b, the 1GNPSS powders shows SS particles that underwent mechanical welding. Near the center of the image are two such welded particles both with a larger particle, a smaller SS particle, and a bridge

between the two. This is reminiscent of grains creating a bridge while fusing together in the initial stages of sintering. Also seen in the images of composite powders are GNPs (yellow circles). The GNPs appear undamaged and dispersed as opposed to agglomerated. Composite powders 2GNPSS (Fig. 2c) and 3GNPSS (Fig. 2d) look the same as 1GNPSS (Fig. 2b) except that the SS particles of 3GNPSS has tiny black spots distributed on the surface. Chemical analysis through energy dispersive spectroscopy was not conducted, so no positive identification could be made. It is thought; however, the spots maybe graphene loosened from GNPs during milling. Smaller GNPs could be seen spread across SS particles in the 2GNPSS powders indicating higher GNP content leads to a higher amount of graphene deposited on the SS particles.

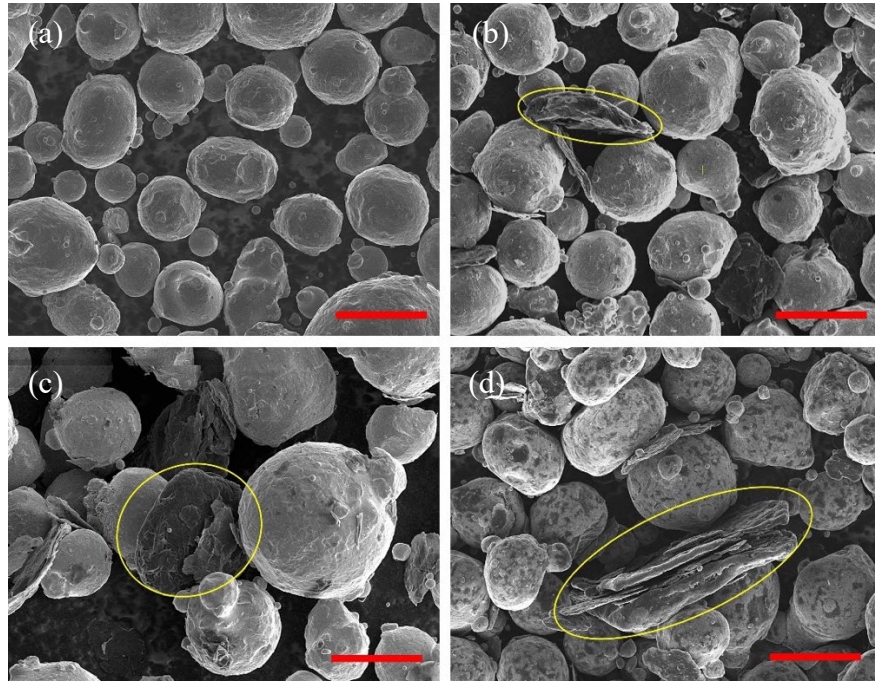


Figure 2. SEM images of powders; (a) pure SS, (b) 1GNP-SS, (c) 2GNP-SS, and (d) 3 GNP-SS. GNPs indicated by yellow circles. Red scale bar is 30 μm .

While printing, some of the composite powders exhibited difficulty in dispensing from the powder hopper. Pure SS and 1GNPSS powders showed no issues, at least due to powder flowability, during printing. A considerable amount of time; however, was spent in resolving clogging issues with the hopper during printing of the 2GNPSS and 3GNPSS powders. Often when using powders with a higher GNP content, the hopper would move across the build plate without dispensing any powder. This was likely caused by powder flowability issues likely due to sufficient agglomeration of GNPs during powder jetting. Evidence for this came in previous work with printing SS with carbon nanotubes (CNT) [9]. When the vol% of CNTs was above 2 vol%, powders would visibly segregate with the black CNTs contrasting sharply with the gray SS powders. These agglomerates would restrict flow of the SS particles. The solution to this problem can be seen in Figure 3. On the outside of the hopper (Fig. 3a), a vibration motor (N20, Tatoko) was attached using resin. On the inside (Fig. 3b), the walls of the hopper were lined with aluminum foil and a second N20 motor was attached to an interior wall. The vibrations from the motor agitate any GNP agglomerations, keeping powder flowing through the open slot at the bottom of the powder hopper. This is like the method of using ultrasonic vibrations to jet highly loaded slurries indirect write

printing [10]. The combination of hoppers and aluminum foil lining the interior walls resolved flow problems encountered with the composite powders.

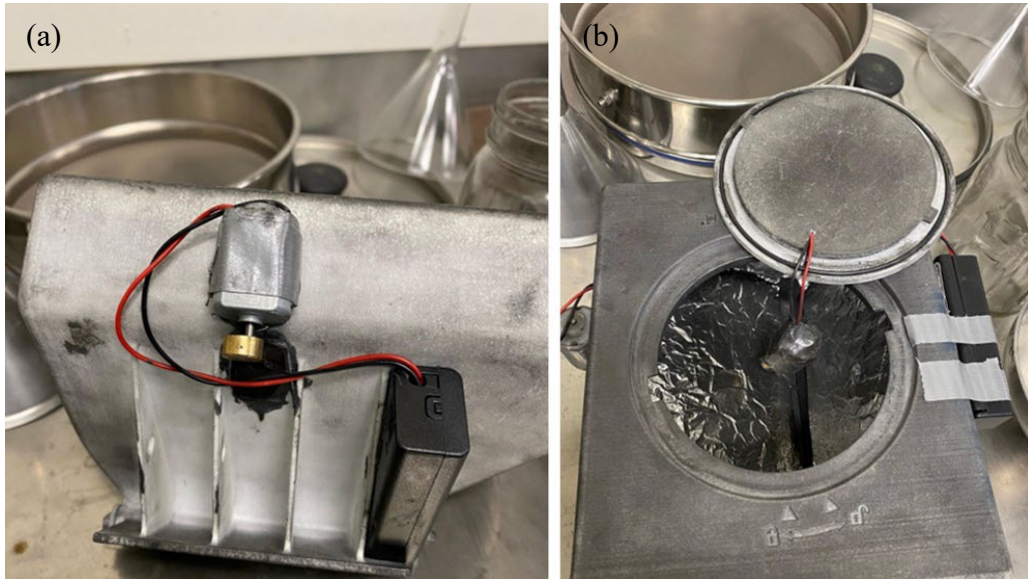


Figure 3. Hopper used for dispensing composite powders. Rumble motor attached to one exterior side (a) of the hopper, and another rumble motor inside (b) the same hopper.

Even after resolving flow issues with the higher GNP content powders, there is still some difficulty in printing composite samples. For the 2GNPSS and 3GNPSS powders, issues persisted with printing at lower energy densities. Continual print failures were encountered at 60 J/mm^3 . As will be seen later, surface roughness and contact angle measurements will be missing for 2GNPSS and 3GNPSS. Despite the difficulties, samples with all loadings of GNP were printed. The cross-sectional microstructure of 3GNPSS samples printed at 67 (Fig. 4a) and 100 J/mm^3 (Fig. 4b) are shown in Figure 4. The typical weld pool pattern seen in LPBF printed metal parts was observed in both samples. It is interesting that the contrast is poor in the 3GNPSS-100 sample as compared to the 3GNPSS-67 sample.

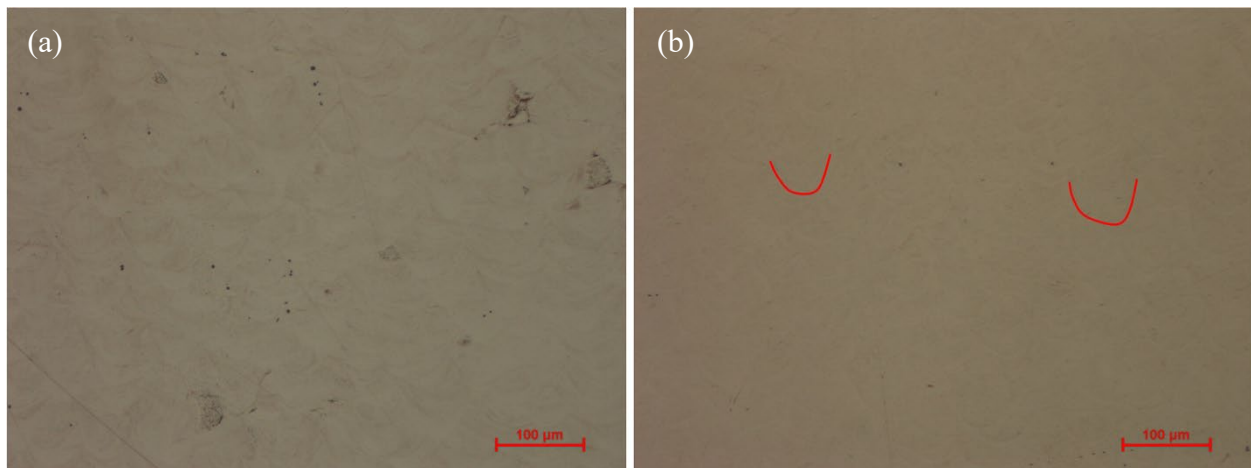


Figure 4. Optical micrographs of the microstructure of printed (a) 3GNPSS-67 and (b) 3GNPSS-100.

Optical profilometry was performed on as-printed surfaces once samples were removed from the build plate. The surface roughness (R_{rms}) in terms of energy density is listed in Table 2. The compositions 2GNPSS and 3GNPSS continued to have issues with failed prints, when printing at 60 J/mm^3 , even after the powder flow issues had been resolved. It is believed that with the lower applied energy and higher GNP loading, enough laser power was absorbed by the GNPs leading to interruption of melt pool formation. So, for 2GNPSS and 3GNPSS, no profilometry or contact angle data exists. The as-printed roughness values fall under columns labeled “ap” while the polished surface roughness values are under “p”.

Table 2. R_{rms} values (in μm) for the as-printed and polished surfaces of samples.

Sample	60 J/mm ³		67 J/mm ³		80 J/mm ³		90 J/mm ³		100 J/mm ³	
	ap	p	ap	p	ap	p	ap	p	ap	p
SS	24.11	0.70	27.80	0.91	17.77	0.55	18.96	0.71	22.24	1.14
1GNPSS	20.73	0.40	25.68	0.41	17.66	0.52	15.15	0.45	15.50	0.32
2GNPSS	-	-	28.91	0.43	19.50	0.48	19.84	0.30	16.55	0.46
3GNPSS	-	-	36.33	1.68	20.85	0.33	22.85	0.27	43.14	0.32

The R_{rms} values of the as-printed surfaces are plotted in the upper portion of each graph in Figure 5 with SS (Fig. 5a), 1GNPSS (Fig. 5b), 2GNPSS (Fig. 5c), and 3GNP SS (Fig. 5d). In the bottom portion of each graph are box & whisker plots of the contact angle measurements taken on the as-printed and polished surfaces of each sample. Also found in each graph is a dotted red line at an angle of 90° . This red line indicates the threshold between hydrophobic and hydrophilic behavior. The surface of 316L stainless-steel typically exhibits weak hydrophilic behavior, i.e., contact angle values are between 80° and 90° [9], [11], [12]. In most cases, as-printed samples exhibited weak hydrophobic behavior. Even the pure as-printed SS samples had contact angles higher than 90° . There was no observed correlation between the measured roughness and the measured contact angles in the as-printed SS samples. The same was true for the 2GNPSS and 3GNPSS samples. For the 1GNPSS samples, there did appear to be a slight increase in the average roughness with a decrease in roughness, which corresponded with an increase energy density of the prints. This may, however, be an exception as generally no changes to contact angle were observed with a change in roughness. It was noted that the roughness values measured from sample to sample were similar.

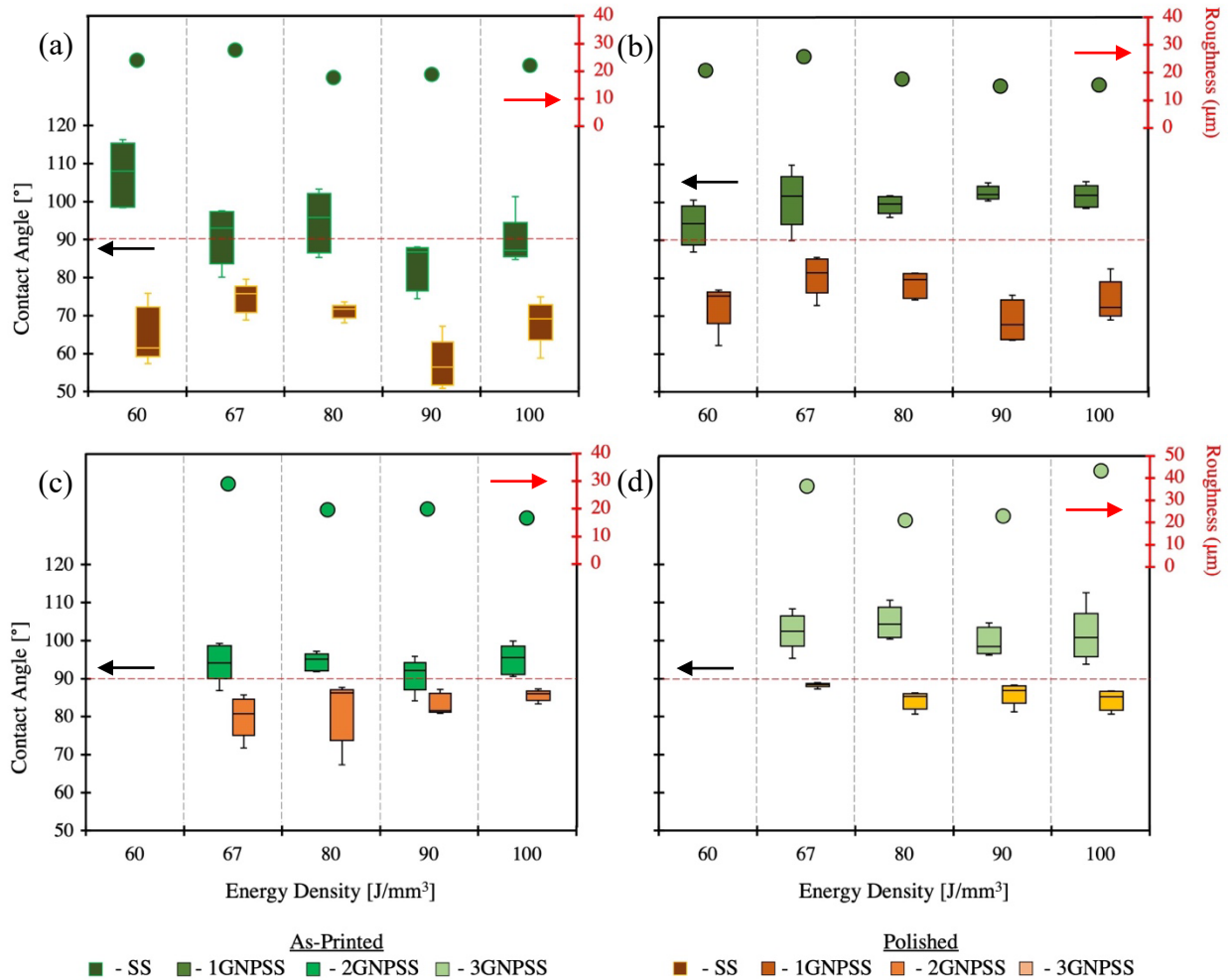


Figure 5. Box and whisker plots of contact angles for as-printed and polished samples: (a) SS, (b) 1GNPSS, (c) 2GNPSS, and (d) 3GNPSS. Dots represent the R_{rms} for the as-printed samples of each composition.

To identify the effect of adding graphene to SS on wetting behavior, as-printed samples were polished, profilometry redone, and contact angles remeasured. The roughness values (Table 2) for the polished surfaces are like the printed surfaces in that there is little change from sample to sample. All polished surfaces showed weak hydrophilic behavior although 3GNPSS-67 exhibited contact angles very near 90° . Contact angles for polished SS samples were all under 80° . The composite 1GNPSS followed the SS with similar wetting behavior. Contact angles closer to 90° were observed for 2GNPSS, especially when printed at 90 and 100 J/mm^3 . Composites with 3 vol% GNP exhibited near hydrophobic behavior with 3GNPSS-67 surfaces with contact angles at 88° . The slight increases in contact angle, at least for the polished surfaces, can be seen in Figure 6. Figures 6a and 6b are examples of water droplets deposited onto as-printed SS-67 and 3GNPSS-67, respectively. Figures 6c and 6d are the polished surfaces of the same samples where it is seen that the contact angles for 3GNPSS-67 are clearly larger than the pure SS-67 polished surface. The data in Figs. 5 and 6 suggest that rough SS surfaces are more inclined toward hydrophobicity as opposed to polished SS surfaces. When composited with GNPs, however, the contact angles of SS tend to increase closer to 90° .

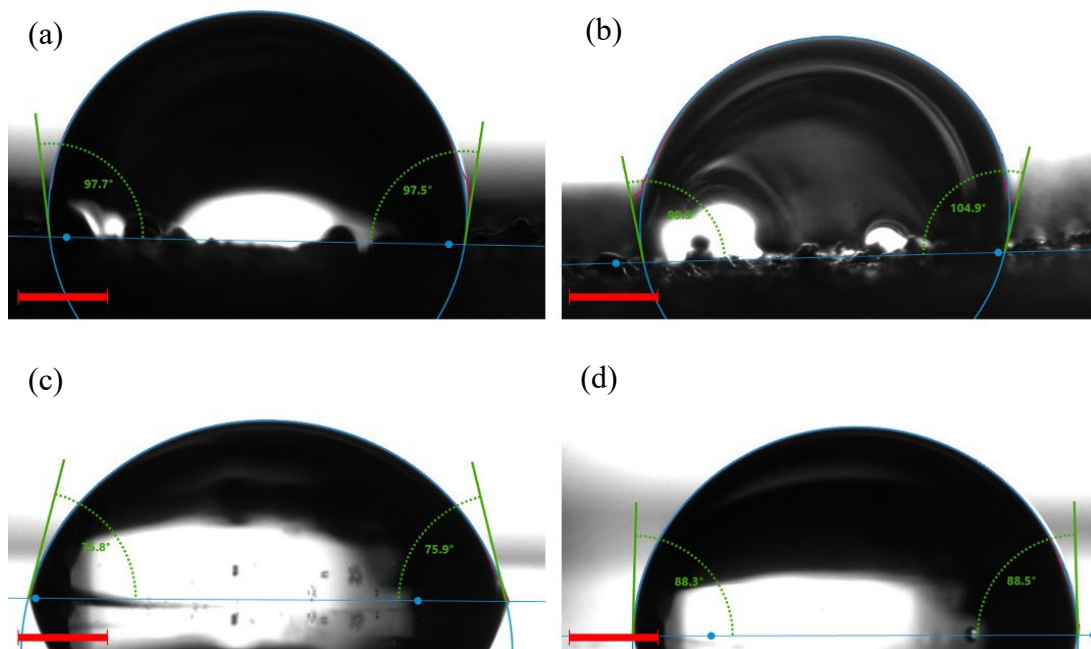


Figure 6. Images of water droplets deposited onto (a) as-printed SS-67, (b) as-printed 3GNP-67, (c) polished SS-67, and (d) polished 3GNP-67. Scale bar is 5 mm.

To corroborate this, an attempt to locate an intact GNP in a printed sample was performed. Printed samples were cut in half for metallurgical examination of the cross-sections. One half was of course polished and etched. The other half was left unpolished and an example for the 3GNPSS sample can be seen in Figure 7. This unpolished surface was cleaned; placed onto a SEM stub; and imaged using the through-the-lens (TL) and annular backscatter (ABS) detectors. The TL detector is a secondary electron detector placed within the beam column and has a higher collection efficiency than the more common Everhart-Thornley detector placed in the chamber. The ABS detector has a higher efficiency for collecting backscatter electrons than the TL detector, which is helpful for compositional contrast imaging. For the 3GNPSS-67 unpolished surface, the TL detector (Fig. 7a) showed black spots distributed across the surface. The ABS detector (Fig. 7b) showed within the larger black spots, dendrites forming within. The contrast seen in the ABS image is likely due mainly to compositional differences between the spot and outside, i.e., darker regions correspond to carbon-rich regions. This suggests these black spots correspond to GNPs and that some reaction occurred between SS and the GNP during printing. The composition of the dendrites is unknown; however, it is reasonable to assume a metal-rich dendrite due to the brighter contrast within the dendrite as compared to the surrounding dark spot.

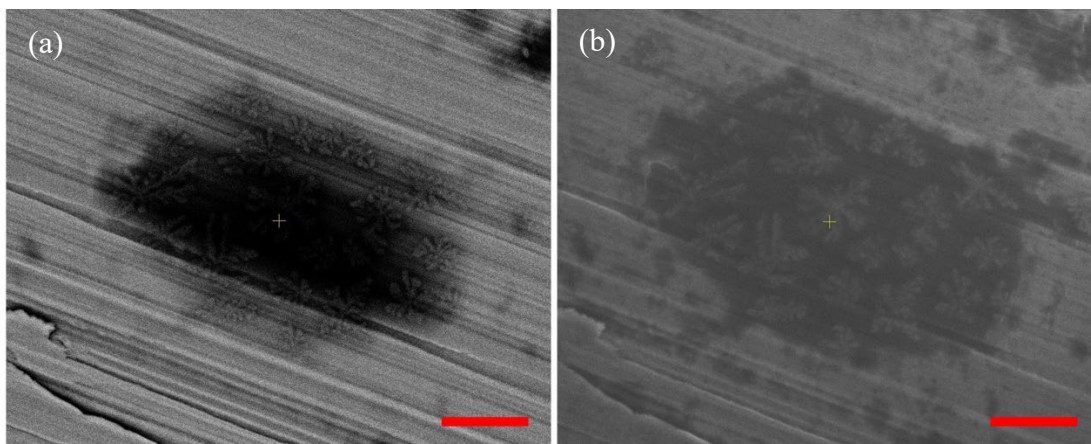


Figure 7. SEM images of the same area of a cut, unpolished cross-section of 3GNPSS-67 with the (a) TL detector and (b) ABS detector.

Conclusions

316L stainless steel composites were printed with graphene nanoplatelets by selective laser melting or laser powder bed fusion. Issues with printing arose with the composites, which included poor to zero powder jetting and lack of fusion. The first issue was addressed by adding a source of vibration to the powder hopper as well as lining the interior of the hopper with aluminum foil to promote powder flow. The other issue was addressed by increasing the energy density above the default setting for 316L SS, 67 Jmm³ with the printer used. As-printed sample surfaces exhibited hydrophobic behavior with contact angles approaching 120°. To study the effect of GNPs on the wetting behavior, printed samples were polished. After polishing the contact angles decreased to hydrophilic angles for all samples printed at all energy densities. The addition of GNPs, however, did lead to small increases to contact angle nearly achieving hydrophobic 90° angles with 3 vol% GNPs. It appeared the GNPs did remain intact during printing but that dendrites appeared to form on the GNPs. Although unexpected, should GNP content increase past the 3 vol%, the dendrites may contribute to pushing contact angles over 90° in the polished composite surfaces. Should these printed SS composites be made hydrophobic, potential applications beyond corrosion resistance may include drag reduction and deicing.

Acknowledgements

The authors would like to thank Dr. Walter Smith for assisting us in the printing of these samples and Dr. Chanman Park for helping us with procurement of argon gas. We would also like to thank the late Dr. Andy Nieto for refining our process.

References

- [1] M. Iannuzzi and G. Frankel, “The carbon footprint of steel corrosion,” *npj Materials Degradation*, vol. 6, no. 1, p. 101, 2022.
- [2] G. A. Jacobson, “NACE international’s IMPACT study breaks new ground in corrosion management research and practice,” *The Bridge*, vol. 46, no. 2, 2016.

- [3] C. Lee, X. Wei, J. W. Kysar, and J. Hone, "Measurement of the elastic properties and intrinsic strength of monolayer graphene," *science*, vol. 321, no. 5887, pp. 385–388, 2008.
- [4] W. Hu *et al.*, "Graphene-based antibacterial paper," *ACS nano*, vol. 4, no. 7, pp. 4317–4323, 2010.
- [5] H. Zhou *et al.*, "Surface deposition of graphene layer for bioactivity improvement of biomedical 316 stainless steel," *Materials Letters*, vol. 192, pp. 123–127, 2017.
- [6] O. Leenaerts, B. Partoens, and F. Peeters, "Water on graphene: Hydrophobicity and dipole moment using density functional theory," *Physical Review B*, vol. 79, no. 23, p. 235440, 2009.
- [7] Y. Song, Y. Liu, H. Jiang, Y. Zhang, Z. Han, and L. Ren, "Biomimetic super hydrophobic structured graphene on stainless steel surface by laser processing and transfer technology," *Surface and Coatings Technology*, vol. 328, pp. 152–160, 2017.
- [8] H. Yin, J. Yang, Y. Zhang, L. Crilly, R. L. Jackson, and X. Lou, "Carbon nanotube (CNT) reinforced 316L stainless steel composites made by laser powder bed fusion: Microstructure and wear response," *Wear*, vol. 496, p. 204281, 2022.
- [9] A. Nieto *et al.*, "3D printed carbon nanotube reinforced stainless steel via selective laser melting," *MRS Communications*, vol. 12, no. 5, pp. 578–584, Oct. 2022, doi: 10.1557/s43579-022-00200-w.
- [10] I. Gunduz, M. McClain, P. Cattani, G.-C. Chiu, J. Rhoads, and S. Son, "3D printing of extremely viscous materials using ultrasonic vibrations," *Additive manufacturing*, vol. 22, pp. 98–103, 2018.
- [11] V. K. Balla, S. Dey, A. A. Muthuchamy, G. Janaki Ram, M. Das, and A. Bandyopadhyay, "Laser surface modification of 316L stainless steel," *Journal of Biomedical Materials Research Part B: Applied Biomaterials*, vol. 106, no. 2, pp. 569–577, 2018.
- [12] S. Cicek, A. Karaca, I. Torun, M. Onses, and B. Uzer, "The relationship of surface roughness and wettability of 316L stainless steel implants with plastic deformation mechanisms," *Materials Today: Proceedings*, vol. 7, pp. 389–393, 2019.